Multi-Agent Conditional Diffusion Model with Mean Field Communication as Wireless Resource Allocation Planner

Kechen Meng, Sinuo Zhang, Rongpeng Li, Xiangming Meng, Chan Wang, Ming Lei, and Zhifeng Zhao

Abstract-In wireless communication systems, efficient and adaptive resource allocation plays a crucial role in enhancing overall Quality of Service (QoS). While centralized Multi-Agent Reinforcement Learning (MARL) frameworks rely on a central coordinator for policy training and resource scheduling, they suffer from scalability issues and privacy risks. In contrast, the Distributed Training with Decentralized Execution (DTDE) paradigm enables distributed learning and decision-making, but it struggles with non-stationarity and limited inter-agent cooperation, which can severely degrade system performance. To overcome these challenges, we propose the Multi-Agent Conditional Diffusion Model Planner (MA-CDMP) for decentralized communication resource management. Built upon the Model-Based Reinforcement Learning (MBRL) paradigm, MA-CDMP employs Diffusion Models (DMs) to capture environment dynamics and plan future trajectories, while an inverse dynamics model guides action generation, thereby alleviating the sample inefficiency and slow convergence of conventional DTDE methods. Moreover, to approximate large-scale agent interactions, a Mean-Field (MF) mechanism is introduced as an assistance to the classifier in DMs. This design mitigates inter-agent non-stationarity and enhances cooperation with minimal communication overhead in distributed settings. We further theoretically establish an upper bound on the distributional approximation error introduced by the MFbased diffusion generation, guaranteeing convergence stability and reliable modeling of multi-agent stochastic dynamics. Extensive experiments demonstrate that MA-CDMP consistently outperforms existing MARL baselines in terms of average reward and QoS metrics, showcasing its scalability and practicality for real-world wireless network optimization.

Index Terms—Wireless communication networks, resource allocation, conditional diffusion model, mean field communication, distribution approximation error analysis of diffusion models.

I. INTRODUCTION

IRELSESS communication networks have been extensively deployed in domains such as smart grids, vehicular communications, and the Internet of Things (IoT) due to their flexibility, low cost, and robustness [1], [2]. Within these networks, efficient resource allocation is vital for optimizing spectrum and energy utilization [3], yet increasing network complexity and the locality of node observations limit system stability and scalability. Traditional rule-based schemes [4], [5] often fail under dynamic or high-load conditions, motivating the use of Reinforcement Learning (RL) for adaptive resource management [6], [7]. However, heterogeneous service

K. Meng, S. Zhang, R. Li, C. Wang, and M. Lei are with the College of Information Science and Electronic Engineering, Zhejiang University (email: {mengkechen, 22431100, lirongpeng, 0617464, lm1029}@zju.edu.cn). X. Meng is with the Zhejiang University-University of Illinois Urbana-Champaign (ZJU-UIUC) Institute, Zhejiang University (e-mail: xiangming-meng@intl.zju.edu.cn). Z. Zhao is with Zhejiang Lab as well as the College of Information Science and Electronic Engineering, Zhejiang University (email: zhaozf@zhejianglab.org).

demands and the dynamic arrival and departure of services often lead to inefficient resource utilization. In response, Multi-Agent RL (MARL) has emerged to further enhance adaptability by enabling distributed decision-making [8], [9]. Existing MARL frameworks primarily follow either the Centralized Training with Decentralized Execution (CTDE) paradigm or the Distributed Training with Decentralized Execution (DTDE) paradigm [10]. While CTDE improves cooperation and credit assignment through centralized training, it suffers from scalability and privacy issues as the number of agents grows [11]. In contrast, DTDE [12], [13] supports fully distributed learning and local collaboration, offering a more scalable solution for large-scale wireless communication networks.

However, DTDE's decentralized structure limits global information sharing, which can exacerbate non-stationarity in multi-agent learning [10]. To improve training stability and sample efficiency, we adopt the Model-Based RL (MBRL) paradigm [14], where a world model is learned from historical logs to simulate potential outcomes and generate synthetic trajectories, enabling agents to exploit past experiences while reducing trial-and-error costs [15]. This formulation treats decision-making as a planning problem, facilitating long-term reasoning and informed policy generation [16]. In essence, the world model serves as a generative model that reconstructs future transitions conditioned on current states and actions. Despite efforts like model ensembling [17] and adversarial learning [18], prediction errors in complex and dynamic wireless networks remain a major challenge. Therefore, improving the generative capability of this model is vital for reliable planning. Recent progress in deep generative modeling offers valuable insights. Compared with earlier approaches such as Energy-Based Models (EBMs) [19], Variational Autoencoders (VAEs) [20], and Generative Adversarial Networks (GANs) [21], Diffusion Models (DMs) demonstrate superior sample quality and training stability through an iterative noiseto-data denoising process, representing the forefront of advances in generative learning [22], [23]. These properties make DMs particularly suitable for offline MBRL. Nevertheless, most MARL algorithms incorporating DMs follow the Model-Free RL (MFRL) paradigm [24], [25], where actions are directly generated by diffusion models, often leading to limited sample utilization and unstable convergence. The integration of DMs with multi-agent MBRL thus remains an open and promising direction for further exploration.

On the other hand, another line of difficulty in DTDE is owing to the lack of a centralized coordinator, which makes the design of communication and fusion mechanisms essential yet challenging [26]. A common approach is the consensus-based method [12], [27], which propagates and aggregates

information through parameterized functions. While its convergence can be theoretically guaranteed under linear function approximation, it becomes unreliable when extended to neural networks. Another research direction employs Graph Neural Networks (GNNs) to model multi-agent interactions and facilitate cooperation through automated relational learning [28], [29]. Although GNN-based methods can capture complex dependencies, they often suffer from high computational costs and heavy data requirements. Compared to these consensus-based or graph-based methods, Mean Field (MF) [30], which allows local information exchange through approximating all other neighbors' dynamics, offers both theoretical performance guarantees and computational efficiency.

In this paper, targeted at addressing the distributed resource allocation mission in wireless communication networks, we propose the Multi-Agent Conditional Diffusion Model Planner (MA-CDMP). Following the DTDE framework for MARL training and execution, we model each network node as an independent agent. For each agent, a diffusion noise model is first employed to model environmental dynamics. Subsequently, an inverse dynamics model maps consecutive observation transitions to corresponding actions, facilitating the derivation of a dynamic resource allocation policy. Prominently, to promote cooperation and efficient communication, we integrate the MF mechanism with the classifier in DM to generate trajectories of high cumulative rewards, where the diffusion-based Stochastic Differential Equation (SDE) models each agent's local observation trajectory together with the averaged observations of its 1-hop neighbors. We theoretically prove that, under MF approximation, the distribution error of diffusion-generated data admits a formal upper bound. It is worth noting that, although related work [31] also combines MF and DMs, their design relies on communicating the global density distribution across all agents, whereas our framework focuses on exchanging averaged local observations within 1hop neighborhoods and leverages a classifier-guided conditional diffusion model for task-specific trajectory generation. Compared with existing literature, the main contributions of this paper can be summarized as follows:

- We propose the MA-CDMP algorithm under the DTDE framework to achieve load-aware resource allocation in wireless communication networks, with each node modeled as an agent. We integrate DMs into the MA-MBRL paradigm for decision generation, leveraging a learned world model to perform conditional planning with improved sample efficiency. Moreover, a MF interaction mechanism is incorporated within the diffusion process to approximate the collective influence of neighboring agents as an aggregated effect, effectively mitigating inter-agent non-stationarity and enhancing coordination in large-scale systems.
- We conduct a theoretical analysis that derives an upper bound on the distribution error of diffusion-generated data under MF communication. Specifically, we first bound the drift term fitting error in the diffusion SDE through MF approximation error analysis. Then, leveraging relative Fisher information [32], we prove that the distribution

TABLE I
MAIN PARAMETERS AND NOTATIONS USED IN THIS PAPER.

Notations	Definition
N	Number of nodes
M	Number of time slots in a frame
L	Number of channels
P_t, P_r	The transmit and received power
G_t, G_r	The antenna gains at the transmitter and receiver
f_c	The carrier frequency
d	The transmission distance
K	Diffusion steps
H	Planning horizon
$\epsilon_{ heta}$	Diffusion noise model
\mathcal{J}_{ψ}	Classifier model
f_{ϕ}	Inverse dynamics model
$egin{array}{c} \mathcal{J}_{\psi} \ f_{\phi} \ \mathcal{N}_{i} \end{array}$	Set of 1-hop neighbors of agent i
$ \begin{array}{c c} f_{\phi} \\ \hline \mathcal{N}_i \\ \hline o_t^{(i)}, a_t^{(i)}, r_t^{(i)} \\ \hline o_t^{(i)} \\ \hline z_t^{(i)} \\ \hline x_k \\ \hline \equiv^{(i)} \\ \end{array} $	Local observation, action and reward of the agent i at t
$\overline{o}_t^{(i)}$	Mean observation over agent i 's 1-hop neighbors at t
$oldsymbol{x}_k^{(i)}$	The observation sequence of agent i at diffusion step k
$\overline{oldsymbol{x}}_k^{(i)}$	Mean observation sequence over agent i 's 1-hop neighbors at diffusion step k
$\widetilde{m{x}}_k^{(i)}$	Concatenated vector of $oldsymbol{x}_k^{(i)}$ and $\overline{oldsymbol{x}}_k^{(i)}$
$oldsymbol{y}^{(i)}$	Conditional signal for agent i
$\operatorname{gen}_t^{(i)}$	Length of packet generation queue at t
$\operatorname{gen}_{\max,t}^{(i)}$	Maximum length of packet generation queue within t
$T_t^{(i)}$	Length of packet transmission queue at t
$T_{\max,t}^{(i)}$	Maximum length of packet transmission queue within t
$d_t^{(i)}$	Time delay of node i at t
ζ	Conditional guidance scale
$L_{\mathcal{J}}, L_{\boldsymbol{\epsilon}}$	Lipschitz constants of the classifier ${\mathcal J}$ and diffusion noise model ϵ

- approximation error of the SDE-based diffusion generative process also admits an explicit upper bound.
- We establish formal performance guarantees for the MA-CDMP algorithm, demonstrating its accuracy and reliability under appropriate parameter configurations. The proposed framework is further evaluated through highfidelity OPNET simulations, demonstrating its superior performance over existing MARL baselines, while extensive ablation studies further validate its robustness, scalability, and adaptability under diverse conditions.

The remainder of the paper is organized as follows. Section II briefly introduces the related works. In Section III, we introduce the preliminaries and formulate the system model. The details of our proposed MA-CDMP algorithm are presented in Section IV, and Section V provides the theoretical analysis establishing its accuracy guarantees. In Section VI, we provide the results of extensive simulations and numerical analysis. Finally, the conclusion is summarized in Section VII.

For convenience, we list the major notations of this paper in Table I.

II. RELATED WORKS

A. Multi-Agent Reinforcement Learning for Resource Scheduling

With the increasing complexity of wireless communication networks and the scarcity of spectrum resources, efficient scheduling is vital for managing channel access and optimizing network utilization. For instance, [6] proposes an actor–critic algorithm to optimize Time Division Multiple Access (TDMA) scheduling and minimize weighted end-to-end delay, while [7] encodes node features into state representations and applies heuristics across time slots to support long-term deadline adherence. However, these methods adopt the single-agent RL paradigm, where centralized control is constrained by limited scalability and the challenge of accurately capturing localized interactions. To address these issues, MARL has gained increasing attention. For instance, [33] develops a load-aware distributed framework for Multi-Frequency TDMA (MF-TDMA) wireless ad hoc networks, defining a network utility function parameterized by traffic loads. QLBT [34] enhances QMIX [35] with an additional per-agent Q-value in the mixing network and integrates delay-to-last-successfultransmission (D2LT) into observations, enabling cooperative policies that prioritize agents with the longest delays. In [36], the authors address impractical power allocation policies in multi-carrier systems and enforce strict compliance with transmit power constraints. Nevertheless, these approaches follow the CTDE paradigm, which requires centralized information aggregation, leading to substantial communication overhead, privacy concerns, and limited expandability in large-scale deployments. In contrast, our work adopts the DTDE framework with MF communication, enabling scalable cooperation among agents with significantly reduced communication cost.

B. Diffusion-Based Resource Allocation in Communication Systems

DMs have achieved remarkable success in various domains, including high-fidelity image synthesis [23], natural language processing [22], and protein structure prediction [37]. Owing to their strong generative capabilities, recent studies have extended DMs to decision-making tasks in RL [38], [39], modeling complex trajectory and action distributions. However, their application in wireless communication networks for resource allocation is still at an early stage. The highly dynamic and complex nature of these networks, coupled with susceptibility to real-world interference, poses significant challenges to the practical deployment of RL algorithms [40]. Several emerging works have integrated DMs into wireless communication tasks targeting these difficulties. For example, [41] proposes a DDPM-based framework that generates optimal block lengths conditioned on channel states. D3PG [42] combines DMs with DDPG [43] to jointly adapt the contention window and aggregation frame length in Wi-Fi networks. Moreover, [44] presents a hierarchical coordination scheme, where a DMenhanced soft actor-critic [45] operates at the high level to produce spectrum allocation strategies, while QMIX [35] functions at the low level for fine-grained power control and resource assignment. Despite promising results, these methods are primarily based on the Model-Free RL (MFRL) paradigm [46], using DMs to directly parameterize the agents' policies. In addition, all adopt the single-agent RL setting—where a centralized coordinator controls the entire network—with [44] employing a single-agent controller at the upper layer. Such designs cannot be directly applied to our MARL scenario and also suffer from low sample efficiency, unstable convergence, and suboptimal decision quality in dynamic and uncertain wireless environments [15]. To overcome these drawbacks, we employ an MBRL-based MARL framework, where DMs approximate the environment's state transition distribution. This modeling strategy enables agents to plan actions without extensive real-world interaction, thereby improving sample efficiency, enhancing convergence stability, and supporting long-horizon planning in complex wireless network scenarios.

C. Diffusion Models for Multi-Agent Reinforcement Learning

Although DMs have demonstrated strong generative capabilities and been applied to decision-making in RL [38], [39], their use in MARL tasks remains limited. Extending DMs to MARL is challenging due to non-stationarity, training instability, and the complexity of modeling inter-agent interactions [47]. To mitigate these limitations, DoF [48] extends the Individual-Global-Max (IGM) [35] principle by introducing a noise factorization function to decompose a centralized diffusion model into agent-specific ones, and a data factorization function to capture dependencies among the generated data. MADiff [49] employs an attention-based diffusion model to learn complex coordination patterns, training a centralized diffusion process for joint trajectory generation while supporting distributed per-agent trajectory generation for teammate modeling. However, these CTDE-based designs still face scalability issues, as the state and action spaces expand exponentially with the number of agents. Motivated by these challenges, another line of research applies DMs within the DTDE framework. For instance, MA-Diffuser [50] extends Diffuser [38] by learning an independent diffusion planner for each agent, with action-value maximization embedded into the sampling process of a conditional diffusion model. DOM2 [24] focuses on overcoming the over-conservatism in offline RL by integrating Conservative Q-Learning (CQL) [51] into Diffusion-QL [52] and introducing a trajectory-based data augmentation strategy to enhance policy diversity and quality. Nevertheless, these independent diffusion models often suffer from poor cooperation among agents. To overcome these limitations, our work adopts the DTDE framework to enhance scalability and integrates MF communication to facilitate inter-agent coordination, enabling efficient and collaborative resource allocation in complex wireless network environments.

D. Theoretical Analysis of Distributional Error in Diffusion-Based Generation

As a class of Score-based Generative Models (SGMs), DMs provide an expressive and efficient framework for modeling complex distributions. Despite their practical success, the theoretical understanding remains incomplete. In particular, [53] establishes Wasserstein distance guarantees for distributions with bounded support or sufficiently decaying tails under L^2 -accurate score estimates, and TV bounds under additional smoothness conditions. However, these results rely on strong assumptions such as the Log-Sobolev Inequality (LSI), and obtaining polynomial-time convergence for multi-modal distributions remains an open problem. Building on different methodologies, [54] employs a Girsanov change-of-measure

framework [55] and analyzes two settings: (i) uniformly Lipschitz-continuous score functions, and (ii) bounded data support. Yet verifying whether the Lipschitz constant scales polynomially with dimension is nontrivial, as it depends on the data distribution's tail behavior. Further, [56] relaxes these assumptions by requiring smoothness only of $\nabla \log p_0$ instead of the entire forward process, thereby sidestepping technical challenges of verifying Novikov's condition [57]. This yields reverse KL guarantees, along with a pure Wasserstein bound that depends on the data distribution's tail decay. Drawing inspiration from these methodologies, our work extends the distributional error analysis to conditional diffusion model and, for the first time, incorporates MF approximation into the theoretical analysis of diffusion processes. Specifically, we analyze the convergence guarantee of conditional diffusion model under MF-guided communication, establishing new theoretical bound on distributional error in multi-agent setting.

III. PRELIMINARIES & SYSTEM MODEL

In this section, we briefly outline the framework of MBRL in multi-agent systems and review the basic principles of DMs. On this basis, we formulate the sequential decision-making problem of resource allocation in wireless communication networks under the DTDE paradigm, integrating DM-based planning with MF-based communication.

A. Preliminaries

1) Multi-Agent Model-Based Reinforcement Learning: We consider a partially observable and fully cooperative multi-agent learning problem, where agents with local observations collaborate to complete the task. This setting is formally described as a Decentralized Partially Observable Markov Decision Process (Dec-POMDP) [58]: G = $\langle \mathcal{S}, \mathcal{O}, \mathcal{A}, P, \mathcal{R}, N, U, \gamma \rangle$, where \mathcal{S} and \mathcal{A} denote state and action space respectively, and γ is the discounted factor. The system contains N agents operating in discrete time steps, starting from an initial global state $s_0 \in \mathcal{S}$ sampled from the distribution U. At each timestep t, agent $i \in \{1, 2, \dots, N\}$ receives a local observation $o_t^{(i)} \in \mathcal{O}^{(i)}$ and selects an action $a_t^{(i)} \in \mathcal{A}^{(i)}$. The joint action $a_t = (a_t^{(1)}, \cdots, a_t^{(N)}) \in \mathcal{A}$ drives the system to the next state s_{t+1} according to the dynamics function $P(s_{t+1}|s_t,a_t): \mathcal{S} \times \mathcal{A} \to \mathcal{S}$, and each agent receives a reward $r_t^{(i)} \in \mathcal{R}$. In offline RL, agents do not interact with the environment directly. Instead, they rely on a static dataset \mathcal{D} , which consists of trajectories \mathcal{T} , i.e., sequences of observations, actions and rewards $\mathcal{T} := \{\{o_0^{(i)}\}_{i=1}^N, \boldsymbol{a}_0, \{r_0^{(i)}\}_{i=1}^N, \{o_1^{(i)}\}_{i=1}^N, \boldsymbol{a}_1, \{r_1^{(i)}\}_{i=1}^N \cdots\}.$ The objective is to learn the optimal joint policy $\boldsymbol{\pi} =$ $(\pi^{(1)}, \cdots, \pi^{(N)})$ from \mathcal{D} so as to maximize the expected cumulative discounted sum of rewards as

$$\boldsymbol{\pi}^* := \arg\max_{\boldsymbol{\pi}} \mathbb{E}_{\mathcal{T} \sim p_{\boldsymbol{\pi}}} \left[\sum_{t \geq 0} \sum_{i=1}^{N} \gamma^t r_t^{(i)} \right]. \tag{1}$$

In MBRL, agents first estimate the dynamics model from collected environmental transition samples. Based on this learned model, they predict future outcomes and conduct planning to optimize the policy [59]. This reduces the need for costly

environment interactions and improves both data efficiency and training stability [15].

2) Diffusion Models: DMs are a class of deep generative models that aim to approximate the unknown data distribution $x_0 \sim p(x)$ from the dataset \mathcal{D} . Instead of directly generating data, DMs define a forward noising process that gradually perturbs data through a predefined Itô SDE [60] as

$$d\mathbf{x}_{\tau} = -\frac{\beta_{\tau}}{2} \mathbf{x}_{\tau} d\tau + \sqrt{\beta_{\tau}} d\mathbf{w}, \qquad (2)$$

where $\beta_{\tau}: \mathbb{R} \to \mathbb{R} > 0$ is the noise schedule, typically taken to be monotonically increasing of the diffusion timestep τ [61], and \boldsymbol{w} is the standard Wiener process. For appropriately chosen β_{τ} and sufficiently large diffuse time T, it is assumed that the distribution converges to a tractable isotropic Gaussian, i.e. $\boldsymbol{x}_T \sim \mathcal{N}(\boldsymbol{0}, \boldsymbol{I})$. The learning objective is to recover the original data distribution by reversing this process, which leads to the reverse SDE [62] as

$$d\boldsymbol{x}_{\tau} = \left[-\frac{\beta_{\tau}}{2} \boldsymbol{x}_{\tau} - \beta_{\tau} \nabla_{\boldsymbol{x}_{\tau}} \log p_{\tau}(\boldsymbol{x}_{\tau}) \right] d\tau + \sqrt{\beta_{\tau}} d\bar{\boldsymbol{w}}, \quad (3)$$

where $d\tau$ corresponds to the diffusion step running backward and $d\bar{\boldsymbol{w}}$ is the reverse Wiener process. The drift term of Eq. (3) depends on the time-dependent score function $\nabla_{\boldsymbol{x}_{\tau}} \log p_{\tau}(\boldsymbol{x}_{\tau})$, which is equivalent to the added noise as

$$\nabla_{\boldsymbol{x}_{\tau}} \log p_{\tau}(\boldsymbol{x}_{\tau}) = -\frac{\boldsymbol{\epsilon}_{\tau}}{\sqrt{1 - \bar{\alpha}_{\tau}}},\tag{4}$$

where we define $\bar{\alpha}_{\tau} := \exp\left(-\int_{0}^{\tau} \beta_{s} \, ds\right)$, and $\epsilon_{\tau} \sim \mathcal{N}(\mathbf{0}, \mathbf{I})$ is the Gaussian noise injected into the dataset sample x_{0} to produce the perturbed sample x_{τ} . Therefore, the reverse denoising process can be learned by optimizing a simplified surrogate objective to predict the added noise ϵ_{τ} as

$$\theta^* = \arg\min_{a} \mathbb{E}_{\tau \sim \mathcal{U}(0,T), \boldsymbol{x}_{\tau} \sim p_{\tau|0}, \boldsymbol{x}_{0} \sim p} \left[\| \boldsymbol{\epsilon}_{\tau} - \boldsymbol{\epsilon}_{\theta}(\boldsymbol{x}_{\tau}) \|^{2} \right], \quad (5)$$

where \mathcal{U} denotes the uniform distribution. With the learned noise function, we can sample data by the reverse denoising SDE in Eq. (3).

To guide DMs toward generating data that satisfies specific conditions, conditional information can be incorporated into the diffusion process. While classifier-free guidance [63] provides a unified parameterization of both conditional and unconditional models, its flexibility is limited under complex constraints. In contrast, classifier guidance [64] has become a widely studied and commonly applied approach [60]. To incorporate conditional information into the generation process, classifier guidance introduces an auxiliary classifier to steer sampling toward desired conditions. Building upon this principle, the conditional distribution can be derived from the unconditional diffusion prior through Bayes' rule as

$$p(\boldsymbol{x}_{\tau} \mid \boldsymbol{y}) = \frac{p(\boldsymbol{x}_{\tau}) p(\boldsymbol{y} \mid \boldsymbol{x}_{\tau})}{p(\boldsymbol{y})}.$$
 (6)

Since p(y) is independent of x_{τ} , Eq. (3) can be modified as

$$d\boldsymbol{x}_{\tau} = \left[-\frac{\beta_{\tau}}{2} \boldsymbol{x}_{\tau} - \beta_{\tau} (\nabla_{\boldsymbol{x}_{\tau}} \log p_{\tau}(\boldsymbol{x}_{\tau}) + \nabla_{\boldsymbol{x}_{\tau}} \log p_{\tau}(\boldsymbol{y} | \boldsymbol{x}_{\tau})) \right] d\tau + \sqrt{\beta_{\tau}} d\bar{\boldsymbol{w}}, \tag{7}$$

Here, the score function $\nabla_{\boldsymbol{x}_{\tau}} \log p_{\tau}(\boldsymbol{x}_{\tau})$ can be obtained from the diffusion noise model optimized in Eq. (5), while the conditional likelihood term $\log p_{\tau}(\boldsymbol{y}|\boldsymbol{x}_{\tau})$ is estimated by an auxiliary network \mathcal{J}_{ψ} . The gradients of \mathcal{J}_{ψ} are then incorporated into the sampling process by modifying the drift term of the reverse dynamics as

$$d\boldsymbol{x}_{\tau} = \left[-\frac{\beta_{\tau}}{2} \boldsymbol{x}_{\tau} + \frac{\beta_{\tau}}{\sqrt{1 - \bar{\alpha}_{\tau}}} \boldsymbol{\epsilon}_{\theta}(\boldsymbol{x}_{\tau}) - \beta_{\tau} \nabla_{\boldsymbol{x}_{\tau}} \mathcal{J}_{\psi}(\boldsymbol{x}_{\tau}) \right] d\tau + \sqrt{\beta_{\tau}} d\bar{\boldsymbol{w}}.$$
(8)

B. System Model

We consider an adaptive, resource-constrained wireless communication network with N nodes, as illustrated in Fig. 1. Each node is modeled as an autonomous agent that makes sequential decisions on resource allocation. In this setup, direct communication is allowed among 1-hop neighbors via wireless transceivers, while remote interactions rely on multihop relaying. The wireless channel follows the Free-Space Path Loss (FSPL) [65] model, where the received power P_r is given by

$$P_r = P_t \cdot G_t \cdot G_r \cdot L_p, \tag{9}$$

with P_t denoting the transmit power and G_t , G_r representing antenna gains at the transmitter and receiver, respectively. The path loss L_p is defined as

$$L_p = \left(\frac{\lambda}{4\pi d}\right)^2,\tag{10}$$

where d is the transmission distance and $\lambda = c/f_c$ is the wavelength, with f_c representing the carrier frequency and c denoting the speed of light. The FSPL model represents an ideal Line-Of-Sight (LOS) propagation environment, providing stable and predictable signal attenuation for accurate performance evaluation. Every node maintains a packet queue for storing generated data, and unacknowledged packets are appended to the end of the cache queue of forwarding nodes. Meanwhile, the network exhibits heterogeneous traffic, where some nodes produce high-rate flows while others generate packets at lower rates, and the imbalance patterns are not known beforehand. To enable efficient spectrum reuse and mitigate inter-node interference, we adopt the MF-TDMA [33] protocol, in which the available resources are partitioned into M orthogonal time slots and L frequency channels, yielding $M \times L$ interference-free Resource Blocks (RBs) per frame. Each transmission frame includes two stages (i.e., network management and traffic transmission). In the first stage, every agent determines its RB demand, which is then normalized to ensure that the total allocation does not exceed $M \times L$. The normalized RBs are then randomly assigned to agents according to their requests. In the second stage, packets are transmitted within the allocated RBs, effectively reducing collision risk and improving spectral efficiency.

We formulate the resource allocation task as a Dec-POMDP [49], and define the decision interval as one frame. Specifically, at each timestep (i.e., one frame) t, agent i obtains a local observation $o_t^{(i)} := \left[\operatorname{gen}_{t}^{(i)}, \operatorname{gen}_{\max,t}^{(i)}, \operatorname{tran}_{t}^{(i)}, \operatorname{tran}_{\max,t}^{(i)} \right]$,

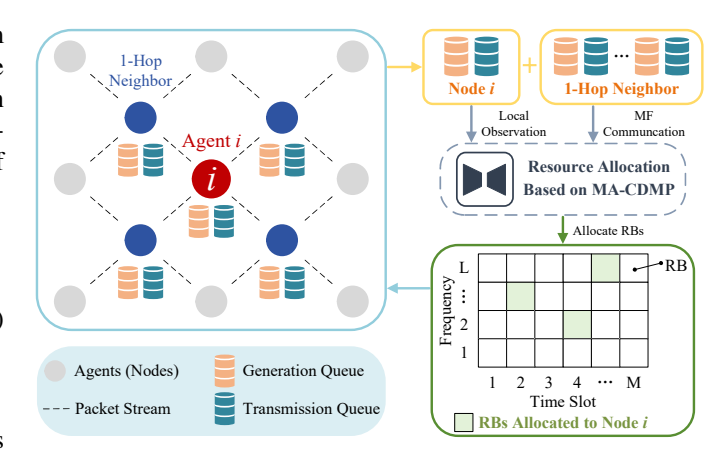


Fig. 1. Overview of the multi-node wireless topology with MF-TDMA-based MAC scheduling.

where $\operatorname{gen}_t^{(i)}$ and $\operatorname{tran}_t^{(i)}$ denote the real-time lengths of the generation and transmission queues, respectively, while $\operatorname{gen}_{\max,t}^{(i)}$ and $\operatorname{tran}_{\max,t}^{(i)}$ represent their corresponding maximum values within frame t. To efficiently enhance coordination under limited communication resources, each agent exchanges local observations with its 1-hop neighbors. As mentioned earlier, many candidate solutions can be employed, such as consensus- [12] or GNN-based aggregation [29] and the MF approximation. In this paper, we leverage the MF approach due to its theoretical guarantees and computational efficiency, capturing the averaged influence as

$$\overline{o}_t^{(i)} := \frac{1}{|\mathcal{N}_i|} \sum_{j \in \mathcal{N}_i} o_t^{(j)}, \tag{11}$$

where \mathcal{N}_i denotes the 1-hop neighbors of agent i. To support long-term decision-making, the action $a_t^{(i)} \in \mathbb{R}$ is generated based on both the local observation sequence and the MF communication sequence, determining the number of RBs requested by the agent. The reward of agent i is defined as

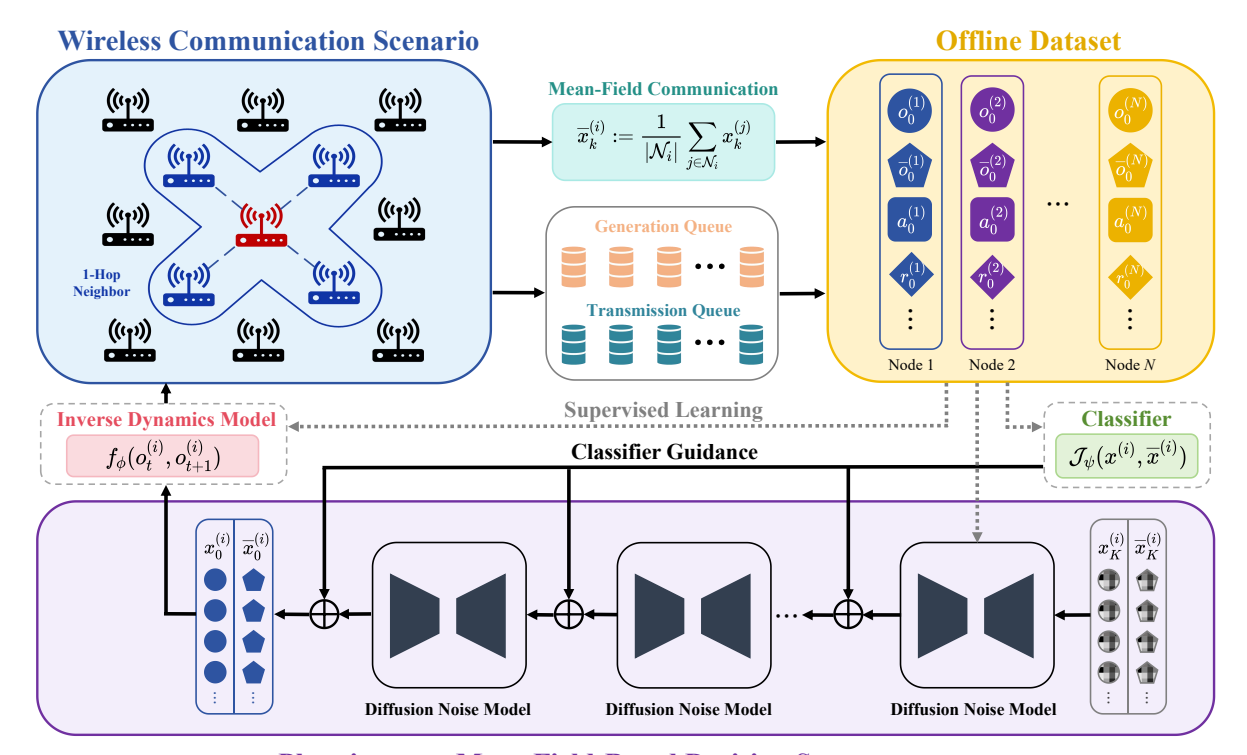
$$r_t^{(i)} := -d_t^{(i)}, (12)$$

where $d_t^{(i)}$ indicates the average time delay for packets received by node i. By minimizing the average delay, we can simultaneously improve throughput and reduce packet loss, thereby enhancing the overall Quality of Service (QoS) without requiring complex weight tuning in multi-objective optimization [66]. In this paper, since nodes exhibit similar structural and operational features, we model them as homogeneous agents.

For each agent i, a policy $\pi^{(i)}$ is learned from its observation sequence and MF communication sequence to collectively maximize the long-term network utility as formulated in Eq. (1). Given the large-scale characteristics of the resource allocation problem in such wireless networks, we devise a distributed MA-CDMP approach with scalable coordination and low communication overhead, laying the foundation for the algorithmic design presented in the following section.

IV. RESOURCE ALLOCATION WITH MA-CDMP

In this section, we discuss how to apply conditional DMs and MF communication to guide the generation of trajectories



Planning over Mean Field-Based Decision Sequence

Fig. 2. The illustration of the MA-CDMP algorithm for resource allocation in wireless communication networks.

with high confidence toward superior cumulative resource allocation rewards. The entire procedure for training and implementation of the proposed MA-CDMP framework is illustrated in Fig. 2.

A. Overview of MA-CDMP

The proposed MA-CDMP encompasses a DM-based dynamics modeling stage, followed by a trajectory-driven planning optimization stage. In the first modeling stage, considering that the discrete and highly fluctuating nature of RB allocation actions increases the difficulty of prediction and modeling, we define $\boldsymbol{x}_k^{(i)}$ as an observation sequence of length H with noise level k, namely

$$\boldsymbol{x}_{k}^{(i)} := (o_{t}^{(i)}, o_{t+1}^{(i)}, \cdots, o_{t+H-1}^{(i)})_{k}.$$
 (13)

Meanwhile, to guide the denoising process toward generating trajectories with high cumulative rewards, the condition $y^{(i)}$ could refer to the return of the trajectory $Return^{(i)}$, that is

$$\mathbf{y}^{(i)} := \text{Return}^{(i)} := \sum_{t'=t}^{t+H-1} \gamma^{t'-t} r_{t'}^{(i)}.$$
 (14)

To this end, we formulate trajectory modeling in MARL as a conditional generative problem based on DMs with classifier guidance [38], namely

$$\max_{\theta, \psi} \mathbb{E}_{\mathcal{T} \sim \mathcal{D}} \left[\log p_{\theta, \psi}(\boldsymbol{x}_0^{(i)} | \boldsymbol{y}^{(i)}) \right]. \tag{15}$$

In this formulation, after characterizing the trajectory distribution $p_{\theta,\psi}$ with the diffusion noise model ϵ_{θ} and the classifier \mathcal{J}_{ψ} , we can generate portions of agent i's trajectory $\boldsymbol{x}_{0}^{(i)}$ conditioned on information $\boldsymbol{y}^{(i)}$. For practical implementation,

we discretize the continuous forward diffusion SDE in Eq. (2) and the reverse denoising SDE in Eq. (7) into K steps, where each diffusion step is indexed by $k \in \{1, \dots, K\}$. Following [61], we denote $\boldsymbol{x}_k := \boldsymbol{x}_{kT/K}$, $\beta_k := \beta_{kT/K}$, and further define $\alpha_k := 1 - \beta_k$, $\bar{\alpha}_k := \prod_{s=1}^k \alpha_s$.

When evaluating trajectories, the classifier operates on the joint observation sequence $\widetilde{x}_k = [x_k^{(1)}, \cdots, x_k^{(N)}]$, as all agents simultaneously make strategic decisions and assess their value functions over the joint trajectory. However, since the dimensionality of \widetilde{x}_k increases exponentially with the number of agents, it's computationally prohibitive to directly model the classifier $\mathcal{J}_{\psi}(\widetilde{x}_k)$. To overcome this challenge, we decompose the classifier into components that rely solely on pairwise local interactions [30] with the agent's 1-hop neighbors as

$$\mathcal{J}_{\psi}(\widetilde{\boldsymbol{x}}_{k}^{(i)}) := \frac{1}{|\mathcal{N}_{i}|} \sum_{j \in \mathcal{N}_{i}} \mathcal{J}_{\psi}(\boldsymbol{x}_{k}^{(i)}, \boldsymbol{x}_{k}^{(j)}). \tag{16}$$

This factorization substantially reduces complexity while still preserving implicit global interactions. The pairwise interaction can be further approximated via MF theory [67], by replacing neighbors with their mean observation as

$$\mathcal{J}_{\psi}(\widetilde{\boldsymbol{x}}_{k}^{(i)}) \sim \mathcal{J}_{\psi}(\boldsymbol{x}_{k}^{(i)}, \overline{\boldsymbol{x}}_{k}^{(i)}), \quad \overline{\boldsymbol{x}}_{k}^{(i)} := \frac{1}{|\mathcal{N}_{i}|} \sum_{i \in \mathcal{N}_{\cdot}} \boldsymbol{x}_{k}^{(j)}. \quad (17)$$

We show that under mild conditions, the approximation error is bounded within a symmetric interval, with the further derivation provided in Section V-A.

Subsequently, given a learned inverse dynamics model $f_{\phi}(o_t^{(i)}, o_{t+1}^{(i)})$ [68], the policy at any timestep t in $x_0^{(i)}$ can be

recovered by estimating the action that leads to the observation transition, namely

$$a_t^{(i)} := f_\phi(o_t^{(i)}, o_{t+1}^{(i)}).$$
 (18)

We leave the details of the training procedure in Section IV-B, while the implementation process of the frameworks will be enumerated in Section IV-C.

B. Training of Core Components in MA-CDMP

Building upon the modeling framework introduced in the previous subsection, we describe the training of the key components that enable effective trajectory-driven planning. Since the agents are modeled as homogeneous, we adopt parameter sharing across agents to enhance efficiency. The classifier $\mathcal{J}_{\psi}(m{x}_k^{(i)}, \overline{m{x}}_k^{(i)})$ is trained in a supervised manner to estimate the cumulative return of a trajectory. To maintain consistency, the diffusion noise model $\epsilon_{\theta}(\boldsymbol{x}_k^{(i)}, \overline{\boldsymbol{x}}_k^{(i)})$ takes both the local observation sequence $\boldsymbol{x}_k^{(i)}$ and the MF observation sequence $\overline{x}_{i}^{(i)}$ as inputs, thereby capturing their joint distribution. In parallel, the inverse dynamics model $f_{\phi}(o_t^{(i)}, o_{t+1}^{(i)})$ is trained under a supervised objective, where the true action $a_t^{(i)}$ serves as the ground-truth signal. Given an offline dataset \mathcal{D} containing observation-action trajectories labeled with rewards, the overall training is conducted by jointly optimizing the classifier loss, reverse diffusion loss, and inverse dynamics loss:

$$\mathcal{L}_{\text{MA-CDMP}}(\psi, \theta, \phi) := \mathbb{E}_{\mathcal{T} \in \mathcal{D}} \left[\| a_t^{(i)} - f_{\phi}(o_t^{(i)}, o_{t+1}^{(i)}) \|^2 \right]$$

$$+ \mathbb{E}_{k, \mathcal{T} \in \mathcal{D}} \left[\| \boldsymbol{\epsilon}_k - \boldsymbol{\epsilon}_{\theta}(\boldsymbol{x}_k^{(i)}, \overline{\boldsymbol{x}}_k^{(i)}) \|^2 \right]$$

$$+ \mathbb{E}_{k, \mathcal{T} \in \mathcal{D}} \left[\| \boldsymbol{y}^{(i)} - \mathcal{J}_{\psi}(\boldsymbol{x}_k^{(i)}, \overline{\boldsymbol{x}}_k^{(i)}) \|^2 \right]$$
(19)

The overall offline training procedure of MA-CDMP is summarized in Algorithm 1.

C. Implementation with MF-Enhanced Classifier Guidance

We implement the well-trained classifier, diffusion noise model, and inverse dynamics model to generate trajectories for policy optimization. Formally, the trajectory generation process begins from Gaussian noise $\left|m{x}_K^{(i)}, \overline{m{x}}_K^{(i)} \right| \sim \mathcal{N}(m{0}, m{I})$ and iteratively refines $\left[\boldsymbol{x}_{k}^{(i)}, \overline{\boldsymbol{x}}_{k}^{(i)}\right]$ into $\left[\boldsymbol{x}_{k-1}^{(i)}, \overline{\boldsymbol{x}}_{k-1}^{(i)}\right]$ at each diffusion step k, with the mean given by

$$\mu_{\theta,\psi} = \frac{1}{\sqrt{\alpha_k}} \left[\left[\mathbf{x}_k^{(i)}, \overline{\mathbf{x}}_k^{(i)} \right] - \frac{1 - \alpha_k}{\sqrt{1 - \bar{\alpha}_k}} \epsilon_{\theta} \left(\left[\mathbf{x}_k^{(i)}, \overline{\mathbf{x}}_k^{(i)} \right] \right) \right] + \zeta \cdot \mathbf{\Sigma}_k \cdot \nabla \mathcal{J}_{\psi} \left(\left[\mathbf{x}_k^{(i)}, \overline{\mathbf{x}}_k^{(i)} \right] \right), \tag{20}$$

where Σ_k denotes the stepwise reverse-diffusion variance prescribed by the sampling schedule (i.e., $\frac{1-\bar{\alpha}_k-1}{1-\bar{\alpha}_k}\beta_k$ in DDPMstyle discretizations [61]), and ζ is a coefficient that balances the influence of the classifier guidance, controlling the strength of conditional enforcement during sampling. In addition, to ensure consistency with the historical data, the first observation of the trajectory is set according to the current state throughout all diffusion steps. After completing K iterations of the denoising process, we can infer the next researchable predicted local Algorithm 1 Offline training of MA-CDMP.

Input: Offline trajectory dataset \mathcal{D} , planning horizon diffusion steps K

Initialize Classifier \mathcal{J}_{ψ} , diffusion noise model ϵ_{θ} and inverse dynamics model f_{ϕ} with random parameters ψ , θ , ϕ

- 1: **for** each epoch **do**
- for each step do 2:
- 3:
- Sample a mini-batch \mathcal{B} of $\boldsymbol{x}_0^{(i)}$ in \mathcal{D} Predict actions $f_{\phi}(o_t^{(i)}, o_{t+1}^{(i)})$ for each observation 4: transition pair in \mathcal{B}
- Compute the MF observation $\overline{x}_0^{(i)}$ by Eq. (17) 5:
- $\mathbf{y}^{(i)} \leftarrow \text{Return}^{(i)}$ 6:
 - ▷ Obtain the condition information by Eq. (14)
- 7: $k \sim \text{Uniform}(\{1, 2, \cdots, K\})$
- 8:

8:
$$\epsilon_k \sim \mathcal{N}(\mathbf{0}, \mathbf{I})$$

9: $\begin{bmatrix} \boldsymbol{x}_k^{(i)}, \overline{\boldsymbol{x}}_k^{(i)} \end{bmatrix} \leftarrow \sqrt{\bar{\alpha}_k} \begin{bmatrix} \boldsymbol{x}_0^{(i)}, \overline{\boldsymbol{x}}_0^{(i)} \end{bmatrix} + \sqrt{1 - \bar{\alpha}_k} \epsilon_k$
 $\triangleright \text{ Apply } \text{ he forward diffusion process}$
0: Predict noise $\epsilon_{\theta}(\boldsymbol{x}_k^{(i)}, \overline{\boldsymbol{x}}_k^{(i)})$

- Predict noise $\epsilon_{\theta}(\boldsymbol{x}_{k}^{(i)}, \overline{\boldsymbol{x}}_{k}^{(i)})$ 10:
- 11:
- Predict return $\mathcal{J}_{\psi}(\boldsymbol{x}_{k}^{(i)}, \overline{\boldsymbol{x}}_{k}^{(i)})$ Update the classifier \mathcal{J}_{ψ} , diffusion noise model ϵ_{θ} 12: and inverse dynamics model f_{ϕ} by Eq. (19)
- end for
- 14: end for

observation and determine the optimal action using our inverse dynamics model f_{ϕ} . This procedure repeats in a standard receding-horizon control loop described in Algorithm 2.

V. ERROR GUARANTEE FOR MA-CDMP

In this section, we focus on the theoretical guarantee for the convergence of the proposed MA-CDMP framework. Specifically, we first analyze the estimation error for the drift term of the diffusion SDE under MF approximation. Building on this, we provide an upper bound on the distributional error of conditional diffusion-based generation.

A. Theoretical Upper Bound on the Drift Term Approximation Error

Consistent with existing literature [30], we first make the following assumptions.

Assumption 1. The classifier \mathcal{J}_{ψ} and diffusion noise model ϵ_{θ} are L-smooth, with gradients that are Lipschitz-continuous with constants $L_{\mathcal{I}}$ and L_{ϵ} , respectively:

$$\|\nabla \mathcal{J}(\boldsymbol{x}^{(i)}, \boldsymbol{x}^{(j)}) - \nabla \mathcal{J}(\boldsymbol{x}^{(i)}, \overline{\boldsymbol{x}}^{(i)})\| \le L_{\mathcal{J}} \|\boldsymbol{x}^{(j)} - \overline{\boldsymbol{x}}^{(i)}\|, \quad (21a)$$

$$\| \nabla \epsilon(\boldsymbol{x}^{(i)}, \boldsymbol{x}^{(j)}) - \nabla \epsilon(\boldsymbol{x}^{(i)}, \overline{\boldsymbol{x}}^{(i)}) \| \le L_{\epsilon} \| \boldsymbol{x}^{(j)} - \overline{\boldsymbol{x}}^{(i)} \|$$
. (21b)

Assumption 2. The difference between observation trajectories is bounded as

$$\|\boldsymbol{x}^{(j)} - \overline{\boldsymbol{x}}^{(i)}\|^2 = \|\boldsymbol{x}^{(j)}\|^2 + \|\overline{\boldsymbol{x}}^{(i)}\|^2 - 2(\boldsymbol{x}^{(j)})^\top \overline{\boldsymbol{x}}^{(i)} \le C, (22)$$

where C is a constant bound related to the magnitude of observation vectors.

Algorithm 2 Implementation of MA-CDMP.

Input: Classifier \mathcal{J}_{ψ} , diffusion noise model ϵ_{θ} , inverse dynamics model f_{ϕ} , planning horizon H, diffusion steps K, conditional guidance scale ζ , number of nodes N, total available RB capacity ML

Initialize $t \leftarrow 0$

Lemma 1. Under Assumptions 1 and 2, for the MF communication mechanism, the drift term approximation error of the reverse-time SDE in Eq. (8) admits an upper bound as

$$\delta_{\text{drift}} \le \frac{CL_{\epsilon}\beta_{\tau}}{\sqrt{1-\bar{\alpha}_{\tau}}} + \sqrt{C}L_{\mathcal{J}}\beta_{\tau}. \tag{23}$$

Proof. Based on the analysis in Appendix B of [69], the MF approximation error admits an upper bound as

$$\parallel \mathcal{J}(\boldsymbol{x}^{(i)}, \overline{\boldsymbol{x}}^{(i)}) - \mathcal{J}(\widetilde{\boldsymbol{x}}^{(i)}) \parallel \leq CL_{\mathcal{J}},$$
 (24)

$$\parallel \epsilon(\boldsymbol{x}^{(i)}, \overline{\boldsymbol{x}}^{(i)}) - \epsilon(\widetilde{\boldsymbol{x}}^{(i)}) \parallel \leq CL_{\epsilon}.$$
 (25)

Next, considering the gradient of the classifier over the observation trajectory, we have

$$\|\nabla \mathcal{J}(\widetilde{\boldsymbol{x}}^{(i)}) - \nabla \mathcal{J}(\boldsymbol{x}^{(i)}, \overline{\boldsymbol{x}}^{(i)}) \|$$

$$= \left\| \frac{1}{|\mathcal{N}_{i}|} \sum_{j \in \mathcal{N}_{i}} \left(\nabla \mathcal{J}(\boldsymbol{x}^{(i)}, \boldsymbol{x}^{(j)}) - \nabla \mathcal{J}(\boldsymbol{x}^{(i)}, \overline{\boldsymbol{x}}^{(i)}) \right) \right\|$$

$$\leq \frac{1}{|\mathcal{N}_{i}|} \sum_{j \in \mathcal{N}_{i}} \|\nabla \mathcal{J}(\boldsymbol{x}^{(i)}, \boldsymbol{x}^{(j)}) - \nabla \mathcal{J}(\boldsymbol{x}^{(i)}, \overline{\boldsymbol{x}}^{(i)}) \|$$

$$\leq \frac{1}{|\mathcal{N}_{i}|} \sum_{j \in \mathcal{N}_{i}} L_{\mathcal{J}} \cdot \| \boldsymbol{x}^{(j)} - \overline{\boldsymbol{x}}^{(i)} \|, \tag{26}$$

where the third line follows from the triangle inequality, while the fourth line applies the Lipschitz-continuity condition in Eq. (21a). With the bounded observation trajectory difference, this yields

$$\|\nabla \mathcal{J}(\widetilde{\boldsymbol{x}}^{(i)}) - \nabla \mathcal{J}(\boldsymbol{x}^{(i)}, \overline{\boldsymbol{x}}^{(i)})\| \le L_{\mathcal{J}}\sqrt{C}. \tag{27}$$

Finally, combining Eq. (25) and Eq. (27), we have the lemma.

B. Theoretical Upper Bound on the SDE-Based Generative Distribution Approximation Error

Theorem 1. Under the MF communication mechanism, the conditional diffusion modeling error between the true initial distribution p_0 and the generated distribution after denoising q_0 is upper bounded as

$$D_{\mathrm{KL}}(p_0 \| q_0) \le \frac{1}{2} M_2 e^{-\bar{\beta}_T} + \frac{1}{2} \int_0^T \mathbb{E}\left[\frac{\delta_{\mathrm{drift}}^2}{\beta_\tau}\right] \mathrm{d}\tau, \tag{28}$$

where we denote $M_2 := \mathbb{E} \| \boldsymbol{x}_t \|^2 < \infty$ as the second-order moment of the data along the SDE, and $\bar{\beta}_T := \int_0^T \beta_\tau \mathrm{d}\tau$.

Before proving Theorem 1, we introduce several key lemmas that establish the necessary theoretical groundwork.

Lemma 2. Consider the Ornstein–Uhlenbeck (OU) process with time-varying coefficient in Eq. (2). The KL divergence between p_T and the standard Gaussian distribution ρ satisfies

$$D_{\mathrm{KL}}(p_T \parallel \rho) \lesssim \frac{1}{2} M_2 \cdot e^{-\bar{\beta}_T}. \tag{29}$$

The proof of Lemma 2 is provided in Appendix A. Notably, this estimate does not depend on the initial distance $D_{\text{KL}}(p_0||\rho)$, as in [54], and further extends the derivation in [56] to the time-varying OU process.

We define the relative Fisher information between p_{τ} and q_{τ} by $J(p_{\tau} \parallel q_{\tau}) = \int p_{\tau}(X_{\tau}) \left\| \nabla \log \frac{p_{\tau}(X_{\tau})}{q_{\tau}(X_{\tau})} \right\|^2 \mathrm{d}X_{\tau}$, and will have the following lemma.

Lemma 3. Consider the following two Itô processes with the same diffusion term $g(\tau)$

$$dX_{\tau} = F_1(X_{\tau}) d\tau + q(\tau) d\boldsymbol{w}, \tag{30}$$

$$dY_{\tau} = F_2(Y_{\tau}) d\tau + g(\tau) d\boldsymbol{w}, \tag{31}$$

where $F_1(X_\tau), F_2(Y_\tau), g(\tau)$ are continuous functions. We assume the uniqueness and regularity condition:

- The two SDEs have unique solutions.
- X_{τ}, Y_{τ} admit densities $p_{\tau}, q_{\tau} \in C^2(\mathbb{R}^d)$ for $T > \tau > 0$.

Then the evolution of $D_{\mathrm{KL}}(p_{\tau} \parallel q_{\tau})$ is given by

$$\frac{\partial}{\partial \tau} D_{\text{KL}}(p_{\tau} \parallel q_{\tau}) = -\frac{1}{2} g(\tau)^{2} J(p_{\tau} \parallel q_{\tau})
+ \mathbb{E} \left[\left\langle F_{1}(X_{\tau}) - F_{2}(X_{\tau}), \nabla \log \frac{p_{\tau}(X_{\tau})}{q_{\tau}(X_{\tau})} \right\rangle \right]. \tag{32}$$

The proof of Lemma 3 is included in Appendix B. Now, we are ready to prove Theorem 1.

Proof. By applying the chain rule of KL divergence, the error can be decomposed as

$$D_{\text{KL}}(p_0||q_0) \le D_{\text{KL}}(p_T||q_T) + \mathbb{E}_{\boldsymbol{x}_T} D_{\text{KL}}(p(\boldsymbol{x}_0|\boldsymbol{x}_T)||q(\boldsymbol{x}_0|\boldsymbol{x}_T)).$$
 (33)

Since the reverse denoising process begins from Gaussian noise, i.e., $q_T \sim \mathcal{N}(\mathbf{0}, \mathbf{I})$, the first term can be bounded by Lemma 2. For the second term in Eq. (33), by applying Lemma 3 and the weighted Young inequality, we yield

$$\frac{\partial}{\partial \tau} D_{\text{KL}}(p_{\tau} \| q_{\tau})
\leq -\frac{\beta_{\tau}}{2} J(p_{\tau} \| q_{\tau}) + \left(\frac{1}{2\beta_{\tau}} \mathbb{E} \| F_{1} - F_{2} \|^{2} + \frac{\beta_{\tau}}{2} J(p_{\tau} \| q_{\tau}) \right)
= \frac{1}{2\beta_{\tau}} \mathbb{E} \| F_{1} - F_{2} \|^{2}.$$
(34)

Integrating both sides of this inequality with respect to τ over the interval [0,T] further yields

$$\mathbb{E}_{\boldsymbol{x}_T} D_{\mathrm{KL}}(p(\boldsymbol{x}_0|\boldsymbol{x}_T) \| q(\boldsymbol{x}_0|\boldsymbol{x}_T)) \leq \int_0^T \mathbb{E}_{\frac{1}{2\beta_\tau}} \| (F_1 - F_2) \|^2 d\tau.$$
(35)

By substituting Eq. (33) and incorporating the upper bound of the drift term error in Lemma 1, we obtain the theorem.

Remark. Theorem 1 establishes that the conditional diffusion modeling error of MA-CDMP under MF communication remains provably bounded. Different from [54], which applies Girsanov's theorem [55] to bound the KL divergence, we employ a differential inequality argument that achieves the same conclusion without such restrictive assumptions. One significant advantage of our derivations is the contingency on a more relaxed and practical assumption: the approach in [54] requires Novikov's condition, which may not always hold. Instead, our analysis depends on a trajectory-smoothness assumption only [56].

Theorem 1 implies that with an appropriate noise schedule and well-trained model parameters, this bound ensures that the approximation error remains controlled, thereby guaranteeing the algorithm's convergence and reliability in modeling the stochastic dynamics of multi-agent communication systems.

VI. PERFORMANCE EVALUATION

In this section, we present numerical experiments to assess the performance and verify the effectiveness of the proposed MA-CDMP framework. We further examine key hyperparameters to characterize their influence and demonstrate robustness.

A. Experimental Settings

We implement the diffusion noise model ϵ_{θ} using a temporal U-Net [70] with 8 residual blocks, organized into 4 down-sampling layers and 4 symmetric up-sampling layers. Timestep and condition embeddings are concatenated and injected into the first temporal convolution of each block. The classifier \mathcal{J}_{ψ} adopts the down-sampling half of this U-Net, with a final linear layer to produce a scalar output. The inverse dynamics model f_{ϕ} is designed as a feed-forward neural network that maps observation transitions to actions. To enhance efficiency and stability, parameters are shared among homogeneous agents.

We employ OPNET as the simulation platform of the wireless communication network. The simulated area spans $10 \text{ km} \times 10 \text{ km}$ with communication nodes randomly distributed. Each node supports 1-hop transmission within a 3.6 km radius and operates over 4 channels at a data rate of 2 Mbps. Each transmission frame consists of 10 time slots. To construct

TABLE II LIST OF KEY PARAMETER SETTINGS FOR THE SIMULATION.

Parameters Description	Value
Number of time slots in a frame	M = 10
Number of channels	L=4
Coverage area of the simulation environment	$10 \text{ km} \times 10 \text{ km}$
1-hop transmission radius of each node	3.6 km
Packet transmission rate	2 Mbps
Communication duration of a trajectory in the offline dataset	30 s
Communication duration of an episode during testing	5 s

the offline dataset with diverse network loads, we configure scenarios with 8 nodes (high- to low-speed ratios of 2:6 and 4:4) and 9 nodes (ratios of 2:7 and 4:5). Packet generation follows an exponential distribution, with the mean arrival time adjusted based on the speed ratio and network topology to ensure load balancing and prevent congestion in dense regions. RBs are allocated according to the high- to low-speed ratio in each scenario. We record the environment data per frame, producing a dataset of 1,000 action-state trajectories labeled with rewards, each corresponding to a communication duration of 30 seconds (i.e., 6,000 timesteps).

To assess the performance of the proposed MA-CDMP algorithm, we follow the evaluation in [71] and extend several state-of-the-art offline RL methods to the multi-agent setting under the DTDE paradigm. The compared baselines include MA-CQL [51], MA-TD3+BC [72], MA-Diffuser [38], MA-DT [73], and MA-DD [39]. To further highlight the effectiveness of our framework, we also compare against MADiff [49], a representative algorithm under the CTDE scheme based on DMs. All methods are trained on the same offline dataset for 100 epochs, epoch comprising 1,000 training steps. During testing, the learned policies are deployed on the OPNET platform under random communication scenarios. Performance is measured over 5-second episodes using the average reward and key QoS metrics, including average throughput, average delay, and packet loss rate. We report the mean and standard deviation across 3 independent scenario seeds to ensure statistical reliability. The key simulation parameters used throughout the experiments are listed in Table II.

B. Numerical Results

1) Performance Comparison: First, to demonstrate the superiority of the proposed MA-CDMP algorithm over other DTDE-based methods, we conduct comparative experiments, as shown in Fig. 3. It can be observed that MA-CDMP achieves higher average rewards after sufficient training and exhibits smoother convergence with smaller reward variance, indicating more stable learning behavior. These results validate the effectiveness of MA-CDMP, showing that the integration of conditional diffusion planning and MF interaction enables more reliable and consistent policy optimization in wireless communication scenarios.

To further evaluate the effectiveness of MA-CDMP, we compare the detailed QoS performance under both ideal and

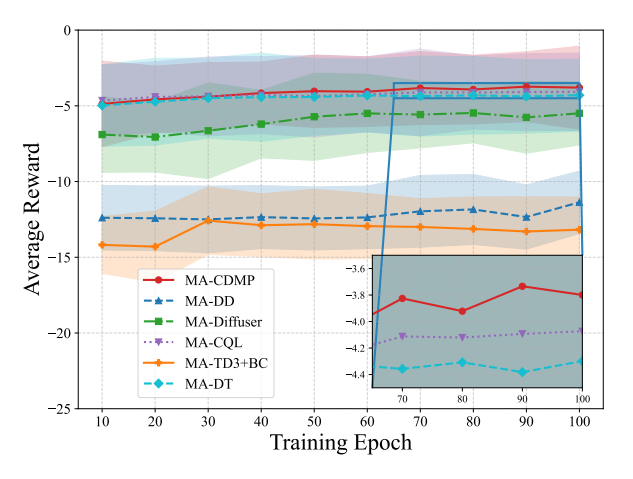


Fig. 3. Comparison of MA-CDMP with other methods in terms of average reward.

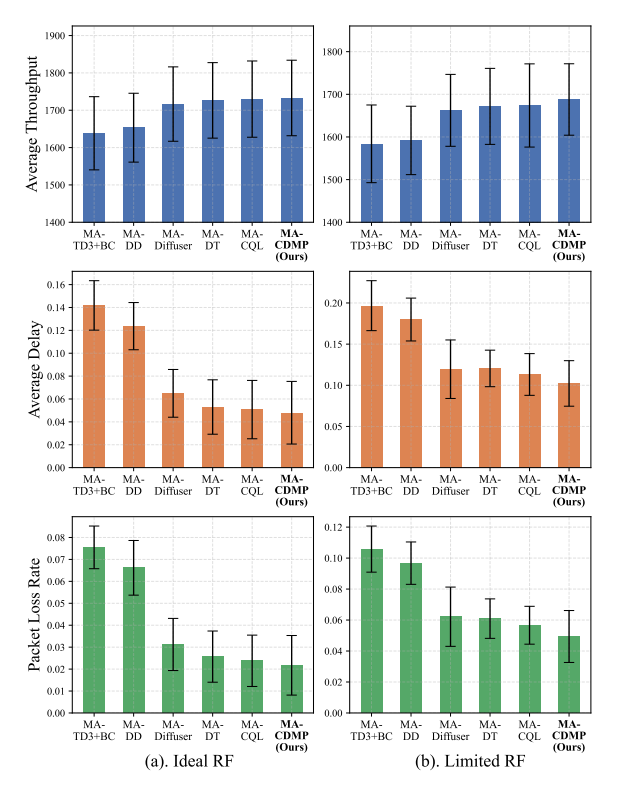


Fig. 4. Comparison of MA-CDMP with other methods in terms of QoS under ideal RF and limited RF scenarios.

limited RF environments, as illustrated in Fig. 4. In the limited RF scenario, the carrier frequency is increased to introduce higher propagation loss, and the transmission power is reduced to emulate shorter communication ranges with degraded signal quality, following the FSPL model in Eq. (9). As shown in the results, although overall performance slightly declines under the limited RF condition, MA-CDMP consistently achieves higher average throughput, lower average delay, and reduced packet loss rate compared with all baselines. These findings verify that MA-CDMP maintains strong adaptability and robustness across varying channel conditions, underscoring its practicality and reliability in complex and dynamic wireless deployment scenarios.

Additionally, we compare the performance of the proposed

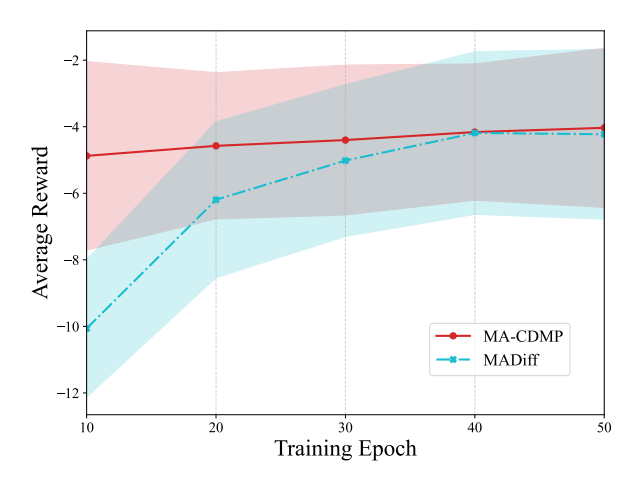


Fig. 5. Comparison of MA-CDMP with MADiff in terms of average reward.

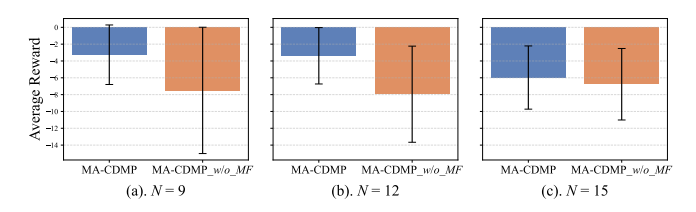


Fig. 6. Comparison of MA-CDMP with MA-CDMP_w/o_MF under varying node number scenarios in terms of average reward.

MA-CDMP algorithm with the CTDE-based MADiff [49] method, as presented in Fig. 5. It can be observed that MA-CDMP achieves faster performance improvement and maintains consistently higher average rewards with smaller variance. These results highlight the advantage of the DTDE paradigm adopted in MA-CDMP, which could yield more stable learning dynamics, ensure better consistency between training and execution, and enhance adaptability in dynamic multi-agent environments.

2) Ablation Studies: To validate the effectiveness of the MF communication mechanism in the MA-CDMP framework, we design a variant that removes this component, denoted as MA-CDMP_w/o_MF, and conduct comparative experiments under different node numbers. As illustrated in Fig. 6, MA-CDMP consistently achieves higher average rewards than MA-CDMP_w/o_MF across all settings. These results highlight the importance of the MF communication mechanism, which facilitates more effective cooperation among agents and enhances overall system performance in wireless environments. Furthermore, MA-CDMP maintains stable and competitive results even as the number of agents increases and when evaluated in previously unseen scenarios, confirming its strong scalability and generalization capability.

Next, to investigate the impact of different planning horizons H on the performance of MA-CDMP, we conduct a comparative experiment as shown in Fig. 7. The results indicate that extending the planning horizon initially improves performance, as a longer horizon enables agents to incorporate more temporal context and make decisions with broader foresight. However, when the horizon becomes excessively long, the performance declines. This degradation arises because the enlarged generative space increases the decision-making

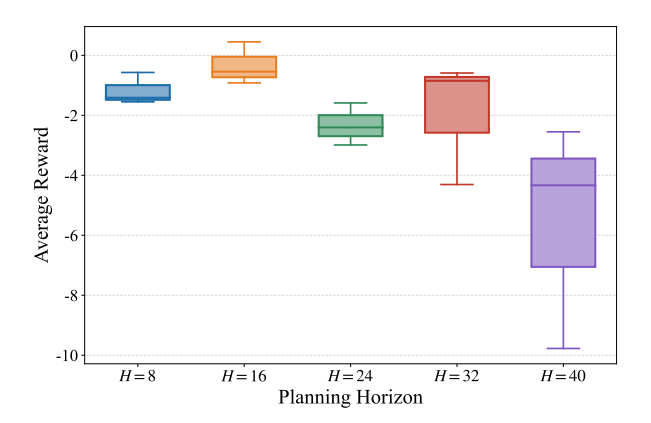


Fig. 7. Comparison of different planning horizons H in terms of average reward.

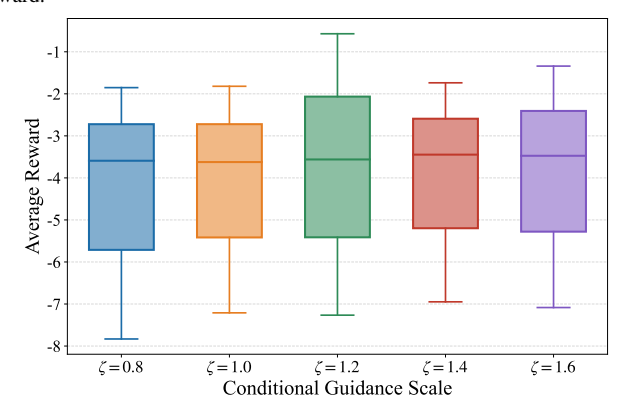


Fig. 8. Comparison of different conditional guidance scales ζ in terms of average reward.

complexity and computational burden, thereby reducing the overall generation efficiency. Hence, in practical deployment, a balanced trade-off between computational cost and algorithmic performance should be carefully maintained.

Furthermore, we investigate how the conditional guidance scale affects the conditional generation capability of the MA-CDMP algorithm. As illustrated in Fig. 8, when the value of ζ increases, the algorithm shows a modest improvement in average reward, yet the overall performance remains relatively consistent. This observation verifies Eq. (20), suggesting that ζ serves as an effective control parameter for regulating the model's ability to generate samples that meet specific conditional constraints. In addition, the stable trend across different ζ values demonstrates the robustness and adaptability of the model with respect to variations in conditional guidance scalar, ensuring reliable results under varying conditions.

We further integrate the DPM-Solver [74] to examine the effect of diffusion step K on the efficiency of decision generation in MA-CDMP. Using a pre-trained noise model with K=100 steps, we apply the first-order DPM-Solver to reduce sampling iterations and evaluate its performance. The results in Fig. 9 show that although reducing diffusion steps leads to a slight decline in performance, MA-CDMP maintains stable average rewards and achieves performance comparable to baseline methods. Moreover, fewer sampling steps significantly lower the computational and time costs, enhancing overall decision-making efficiency. In practical deployments, K can be flexibly adjusted to balance performance

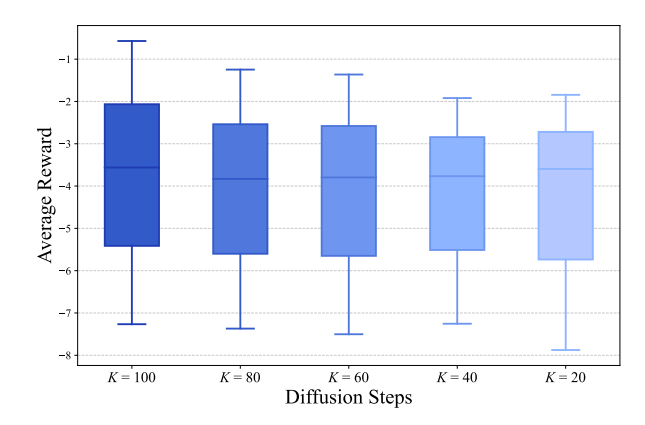


Fig. 9. Comparison of different diffusion steps K in terms of average reward.

and computational demand according to specific deployment requirements.

VII. CONCLUSION

In this paper, we have investigated distributed resource allocation in multi-node, resource-constrained wireless communication networks. Under the MBRL paradigm, we have proposed the MA-CDMP algorithm, which significantly improves communication efficiency and system performance. Specifically, we have employed a conditional diffusion model to predict local observation sequences with high cumulative rewards and utilized an inverse dynamics model to generate corresponding actions. To enable cooperative behavior among distributed nodes and optimize global performance, we have integrated MF communication to enhance the performance of classifer-based world modeling. Moreover, we have theoretically established an upper bound on the discrepancy between the diffusion-generated distribution under MF approximation and the true distribution. Extensive simulations have confirmed the effectiveness, robustness, and scalability of the proposed algorithm.

APPENDIX A PROOF FOR LEMMA 2

Based on Itô's Lemma [75], the first-order linear SDE with time-varying coefficients admits the closed-form solution as

$$p_T(\boldsymbol{x}_T|\boldsymbol{x}_0) = \mathcal{N}\left(e^{-\frac{1}{2}\bar{\beta}_T}\boldsymbol{x}_0, \left(1 - e^{-\bar{\beta}_T}\right)\boldsymbol{I}\right).$$
 (36)

To bound the divergence between p_T and the standard Gaussian ρ , we apply Jensen's inequality, which yields

$$D_{KL}(p_T \parallel \rho) = D_{KL} \left(\int p_T(\boldsymbol{x}_T | \boldsymbol{x}_0) \, p_0(\boldsymbol{x}_0) d\boldsymbol{x}_0 \parallel \rho \right)$$

$$\leq \mathbb{E}_{\boldsymbol{x}_0 \sim p_0} [D_{KL}(p_T(\boldsymbol{x}_T | \boldsymbol{x}_0) \parallel \rho)]. \tag{37}$$

For a d-dimensional Gaussian distribution $\mathcal{N}(\pmb{\mu}, \pmb{\Sigma})$, the KL divergence with respect to ρ has a closed form as

$$D_{\text{KL}}(\mathcal{N}(\boldsymbol{\mu}, \boldsymbol{\Sigma}) \| \rho) = \frac{1}{2} \left(\text{Tr}(\boldsymbol{\Sigma}) - d - \text{logdet}(\boldsymbol{\Sigma}) + \| \boldsymbol{\mu} \|^2 \right).$$
 (38)

Substituting the mean and covariance from Eq. (36), we obtain

$$D_{\text{KL}}(p_T \| \rho) = \frac{1}{2} \left[-d \log \left(1 - e^{-\bar{\beta}_T} \right) - d e^{-\bar{\beta}_T} + e^{-\bar{\beta}_T} \| \boldsymbol{x}_0 \|^2 \right]. \tag{39}$$

Taking expectation over $x_0 \sim p_0$ and using the second-order moment M_2 , Eq. (37) leads to

$$D_{\text{KL}}(p_T \| \rho) \leq \mathbb{E}_{p_0} \left[\frac{1}{2} \left(-d \log(1 - e^{-\bar{\beta}_T}) - de^{-\bar{\beta}_T} + e^{-\bar{\beta}_T} \| \boldsymbol{x}_0 \|^2 \right) \right]$$

$$= \frac{1}{2} \left[-d \log(1 - e^{-\bar{\beta}_T}) - de^{-\bar{\beta}_T} + M_2 e^{-\bar{\beta}_T} \right]. \tag{40}$$

Finally, under appropriately designed noise schedule, $e^{-\bar{\beta}_T}$ becomes sufficiently small. Applying the first-order approximation $\log(1-e^{-\bar{\beta}_T})\approx -e^{-\bar{\beta}_T}$, we derive

$$D_{\mathrm{KL}}(p_T \parallel \rho) \lesssim \frac{1}{2} M_2 \, e^{-\bar{\beta}_T}. \tag{41}$$

Then the lemma comes.

APPENDIX B PROOF FOR LEMMA 3

By the Fokker-Planck equation [76], the evolution of p_{τ} and q_{τ} is given by

$$\frac{\partial p_{\tau}}{\partial \tau}(X_{\tau}) = \nabla \left[-F_1(X_{\tau})p_{\tau}(X_{\tau}) + \frac{g(\tau)^2}{2} \nabla p_{\tau}(X_{\tau}) \right], \quad (42)$$

$$\frac{\partial q_{\tau}}{\partial \tau}(X_{\tau}) = \nabla \left[-F_2(X_{\tau})q_{\tau}(X_{\tau}) + \frac{g(\tau)^2}{2} \nabla q_{\tau}(X_{\tau}) \right]. \quad (43)$$

Consequently, we can write

$$\frac{\partial}{\partial \tau} D_{\text{KL}}(p_{\tau} \| q_{\tau}) = \int \log \frac{p_{\tau}}{q_{\tau}} \frac{\partial p_{\tau}}{\partial \tau} dX_{\tau} - \int \frac{p_{\tau}}{q_{\tau}} \frac{\partial q_{\tau}}{\partial \tau} dX_{\tau}. \tag{44}$$

For the first term, substituting $\frac{\partial p_{\tau}}{\partial \tau}$ and applying integration by parts under the assumption that the boundary term vanishes (i.e., the probability flux at infinity is zero), we obtain

$$\int \log \frac{p_{\tau}}{q_{\tau}} \frac{\partial p_{\tau}}{\partial \tau} dX_{\tau} = \int \nabla \left[-F_{1} p_{\tau} + \frac{g(\tau)^{2}}{2} \nabla p_{\tau} \right] \log \frac{p_{\tau}}{q_{\tau}} dX_{\tau}
= \int \left\langle \nabla \log \frac{p_{\tau}}{q_{\tau}}, F_{1} p_{\tau} - \frac{g(\tau)^{2}}{2} \nabla p_{\tau} \right\rangle dX_{\tau}
= \int p_{\tau} \left\langle F_{1}, \nabla \log \frac{p_{\tau}}{q_{\tau}} \right\rangle dX_{\tau} - \int \frac{g(\tau)^{2}}{2} \left\langle \nabla \log \frac{p_{\tau}}{q_{\tau}}, \nabla p_{\tau} \right\rangle dX_{\tau}.$$
(45)

Similarly, the second term yields

$$\int \frac{p_{\tau}}{q_{\tau}} \frac{\partial q_{\tau}}{\partial \tau} dX_{\tau} = \int \frac{p_{\tau}}{q_{\tau}} \nabla \left[-F_{2}q_{\tau} + \frac{g(\tau)^{2}}{2} \nabla q_{\tau} \right] dX_{\tau}$$

$$= \int \left\langle \nabla \frac{p_{\tau}}{q_{\tau}}, F_{2}q_{\tau} - \frac{g(\tau)^{2}}{2} \nabla q_{\tau} \right\rangle dX_{\tau}$$

$$= \int q_{\tau} \left\langle \nabla \frac{p_{\tau}}{q_{\tau}}, F_{2} \right\rangle dX_{\tau} - \frac{g(\tau)^{2}}{2} \int \left\langle \nabla \frac{p_{\tau}}{q_{\tau}}, \nabla q_{\tau} \right\rangle dX_{\tau}. \tag{46}$$

Notice that

$$\int \left\langle \nabla \frac{p_{\tau}}{q_{\tau}}, \nabla q_{\tau} \right\rangle dX_{\tau} - \int \left\langle \nabla \log \frac{p_{\tau}}{q_{\tau}}, \nabla p_{\tau} \right\rangle dX_{\tau}
= \int \left\langle \frac{q_{\tau} \nabla p_{\tau} - p_{\tau} \nabla q_{\tau}}{q_{\tau}}, \nabla \log q_{\tau} \right\rangle dX_{\tau} - \int p_{\tau} \left\langle \nabla \log \frac{p_{\tau}}{q_{\tau}}, \nabla \log p_{\tau} \right\rangle dX_{\tau}
= \int p_{\tau} \left\langle \nabla \log \frac{p_{\tau}}{q_{\tau}}, \nabla \log q_{\tau} \right\rangle dX_{\tau} - \int p_{\tau} \left\langle \nabla \log \frac{p_{\tau}}{q_{\tau}}, \nabla \log p_{\tau} \right\rangle dX_{\tau}
= -J(p_{\tau} || q_{\tau}),$$
(47)

and

$$\begin{split} &\int p_{\tau} \left\langle F_{1}, \nabla \log \frac{p_{\tau}}{q_{\tau}} \right\rangle \mathrm{d}X_{\tau} - \int q_{\tau} \left\langle \nabla \frac{p_{\tau}}{q_{\tau}}, F_{2} \right\rangle \mathrm{d}X_{\tau} \\ &= \int p_{\tau} \left\langle F_{1}, \nabla \log \frac{p_{\tau}}{q_{\tau}} \right\rangle \mathrm{d}X_{\tau} - \int p_{\tau} \left\langle \nabla \log \frac{p_{\tau}}{q_{\tau}}, F_{2} \right\rangle \mathrm{d}X_{\tau} \\ &= \int p_{\tau} \left\langle \nabla \log \frac{p_{\tau}}{q_{\tau}}, F_{1} - F_{2} \right\rangle \mathrm{d}X_{\tau} \end{split}$$

$$= \mathbb{E}\left[\left\langle F_1 - F_2, \nabla \log \frac{p_\tau}{q_\tau} \right\rangle\right]. \tag{48}$$

Therefore, the lemma follows.

REFERENCES

- [1] M. Alsabah, et al., "6g wireless communications networks: A comprehensive survey," *IEEE Access*, vol. 9, pp. 148191–148243, 2021.
- [2] J. Q. Kadhim, et al., "Enhancement of online education in engineering college based on mobile wireless communication networks and iot," Int. J. Emerg. Technol. Learn. (Online), vol. 18, no. 1, p. 176, 2023.
- [3] S. Aboagye, et al., "Multi-band wireless communication networks: Fundamentals, challenges, and resource allocation," *IEEE Trans. Commun.*, vol. 72, no. 7, pp. 4333–4383, 2024.
- vol. 72, no. 7, pp. 4333–4383, 2024.

 [4] B. Suman, et al., "A dynamic tdma slot scheduling(dtss) scheme for efficient channel allocation in tactical ad hoc networks," in Proc. IEEE Int. Conf. Comput. Commun. Automat. (ICCCA), Noida, India, May 2015, pp. 815–838.
- [5] I. Jabandžić, et al., "A dynamic distributed multi-channel tdma slot management protocol for ad hoc networks," *IEEE Access*, vol. 9, pp. 61 864–61 886, Apr 2021.
- [6] G. Wi, et al., "Delay-aware tdma scheduling with deep reinforcement learning in tactical manet," in Int. Conf. Inf. Commun. Tech. Conv. (ICTC), Jeju, Korea, Oct 2020, pp. 370–372.
- [7] S. Chilukuri, et al., "Deadline-aware tdma scheduling for multihop networks using reinforcement learning," in IFIP Net. Conf., Espoo and Helsinki, Finland, Jun 2021, pp. 1–9.
- [8] M. Sohaib, et al., "Dynamic multichannel access via multi-agent reinforcement learning: Throughput and fairness guarantees," IEEE Trans. Wireless Commun., vol. 21, no. 6, pp. 3994–4008, 2021.
- [9] L. Miuccio, et al., "On learning generalized wireless mac communication protocols via a feasible multi-agent reinforcement learning framework," *IEEE Trans. Mach. Learn. Commun. Networking*, vol. 2, pp. 298–317, 2024.
- [10] S. Hwang, et al., "Decentralized computation offloading with cooperative uavs: Multi-agent deep reinforcement learning perspective," *IEEE Wireless Commun.*, vol. 29, no. 4, pp. 24–31, 2022.
- [11] K. Xu, et al., "Distributed-training-and-execution multi-agent reinforcement learning for power control in hetnet," *IEEE Trans. Commun.*, vol. 71, no. 10, pp. 5893–5903, Oct 2023.
- [12] Z. Chen, et al., "Sample and communication-efficient decentralized actor-critic algorithms with finite-time analysis," in Proc. Int. Conf. Mach. Learn. (ICML), Baltimore, Maryland, USA, Jul 2022, pp. 3794– 3834.
- [13] K. Li, et al., "Multi-agent reinforcement learning with decentralized distribution correction," *IEEE Trans. Autom. Sci. Eng.*, vol. 22, pp. 1684– 1696, Feb 2024.
- [14] T. M. Moerland, et al., "Model-based reinforcement learning: A survey," Found. Trends Mach. Learn., vol. 16, no. 1, pp. 1–118, 2023.
- [15] Q. Huang, "Model-based or model-free, a review of approaches in reinforcement learning," in *Proc. Int. Conf. Comput. Data Sci. (ICCDS)*, Stanford, CA, USA, Aug 2020, pp. 219–221.
- [16] C. You, et al., "Advanced planning for autonomous vehicles using reinforcement learning and deep inverse reinforcement learning," Rob. Auton. Syst., vol. 114, pp. 1–18, Apr 2019.
- [17] K. Chua, et al., "Deep reinforcement learning in a handful of trials using probabilistic dynamics models," in Proc. Adv. Neural Inf. Proces. Syst. (NeurIPS), Montréal, Canada, Dec 2018, pp. 4759–4770.
- [18] F.-M. Luo, et al., "Reward-consistent dynamics models are strongly generalizable for offline reinforcement learning," arXiv preprint arXiv:2310.05422, 2023.
- [19] Y. Du, et al., "Implicit generation and modeling with energy based models," in Proc. Adv. Neural Inf. Proces. Syst. (NeurIPS), Vancouver, Canada, Dec 2019, pp. 3608–3618.
- [20] D. P. Kingma, et al., "Auto-encoding variational bayes," in Proc. Int. Conf. Learn. Represent. (ICLR), Scottsdale, Arizona, USA, May 2013.
- [21] I. Goodfellow, et al., "Generative adversarial nets," in Proc. Adv. Neural Inf. Proces. Syst. (NeurIPS), Montréal, Canada, Dec 2014, pp. 73–76.
- [22] T. Brown, et al., "Language models are few-shot learners," in Proc. Adv. Neural Inf. Proces. Syst. (NeurIPS), Virtual Edition, Dec 2020, pp. 1877–1901.
- [23] R. Rombach, et al., "High-resolution image synthesis with latent diffusion models," in Proc. IEEE Conf. Comput. Vis. Pattern Recognit. (CVPR), New Orleans, LA, USA, Jun 2022, pp. 10674–10685.
- [24] Z. Li, et al., "Beyond conservatism: Diffusion policies in offline multiagent reinforcement learning," arXiv preprint arXiv:2307.01472, 2023.

- [25] Z. Liu, et al., "Dnn partitioning, task offloading, and resource allocation in dynamic vehicular networks: A lyapunov-guided diffusion-based reinforcement learning approach," *IEEE Trans. Mob. Comput.*, pp. 1–17, Oct 2024.
- [26] G. Qu, et al., "Scalable reinforcement learning for multiagent networked systems," Oper. Res., vol. 70, no. 6, pp. 3601–3628, 2022.
- [27] C. Qu, et al., "Value propagation for decentralized networked deep multi-agent reinforcement learning," in Proc. Adv. Neural Inf. Proces. Syst. (NeurIPS), Vancouver, Canada, Dec 2019.
- [28] J. Blumenkamp, et al., "The emergence of adversarial communication in multi-agent reinforcement learning," in Proc. Conf. Robot Learn. (CoRL), London, UK, Nov 2021.
- [29] S. Nayak, et al., "Scalable multi-agent reinforcement learning through intelligent information aggregation," in Proc. Int. Conf. Mach. Learn. (ICML), Honolulu, Hawaii, USA, Jul 2023, pp. 25817–25833.
- [30] Y. Yang, et al., "Mean field multi-agent reinforcement learning," in Proc. Int. Conf. Mach. Learn. (ICML), Stockholm, Sweden, Jul 2018, pp. 5571–5580
- [31] W. Yuan, et al., "Integrating mean-field game theory with diffusion model," in Proc. IEEE SPAWC 2025, Surrey, UK, Jul 2025.
- [32] K. Sun, et al., "Relative fisher information and natural gradient for learning large modular models," in Proc. Int. Conf. Mach. Learn. (ICML), Sydney, Australia, Aug 2017, pp. 3289–3298.
- [33] S. Zhang, et al., "Load-aware distributed resource allocation for mf-tdma ad hoc networks: A multi-agent drl approach," *IEEE Trans. Network Sci.* Eng., vol. 9, no. 6, pp. 4426–4443, Aug 2022.
- [34] Z. Guo, et al., "Multi-agent reinforcement learning-based distributed channel access for next generation wireless networks," *IEEE J. Sel. Areas Commun.*, vol. 40, no. 5, pp. 1587–1599, 2022.
- [35] T. Rashid, et al., "Monotonic value function factorisation for deep multiagent reinforcement learning," J. Mach. Learn. Res., vol. 21, no. 1, pp. 7234–7284, Jan 2020.
- [36] A. Kopic, et al., "A collaborative multi-agent deep reinforcement learning-based wireless power allocation with centralized training and decentralized execution," *IEEE Trans. Commun.*, vol. 72, no. 11, pp. 7006–7016, 2024.
- [37] J. Watson, et al., "De novo design of protein structure and function with rfdiffusion," Nature, vol. 620, 07 2023.
- [38] M. Janner, et al., "Planning with diffusion for flexible behavior synthesis," in Proc. Int. Conf. Mach. Learn. (ICML), Baltimore, Maryland, USA, Jul 2022, pp. 9902–9915.
- [39] A. Ajay, et al., "Is conditional generative modeling all you need for decision-making?" in Proc. Int. Conf. Learn. Represent. (ICLR), Kigali, Rwanda, May 2023, pp. 29598–29620.
- [40] Y. Liu, et al., "Deep generative model and its applications in efficient wireless network management: A tutorial and case study," *IEEE Wireless Commun.*, vol. 31, no. 4, pp. 199–207, Aug 2024.
- [41] A. Babazadeh Darabi, et al., "Diffusion model based resource allocation strategy in ultra-reliable wireless networked control systems," IEEE Commun. Lett., vol. 29, no. 1, pp. 85–89, Jan 2025.
- [42] T. Liu, et al., "Generative diffusion model (gdm) for optimization of wi-fi networks," arXiv preprint arXiv:2404.15684, 2024.
- [43] T. P. Lillicrap, et al., "Continuous control with deep reinforcement learning," in Proc. Int. Conf. Learn. Represent. (ICLR), Caribe Hilton, San Juan, Puerto Rico, May 2016.
- [44] P. Ning, et al., "Diffusion-based deep reinforcement learning for resource management in connected construction equipment networks: A hierarchical framework," *IEEE Trans. Wireless Commun.*, vol. 24, no. 4, pp. 2847–2861, Jan 2025.
- [45] T. Haarnoja, et al., "Soft actor-critic: Off-policy maximum entropy deep reinforcement learning with a stochastic actor," in Proc. Int. Conf. Mach. Learn. (ICML), Stockholm, Sweden, Jul 2018, pp. 1861–1870.
- [46] J. Ramírez, et al., "Model-free reinforcement learning from expert demonstrations: a survey," Artif. Intell. Rev., vol. 55, no. 4, pp. 3213– 3241, 2022.
- [47] J. Chen, et al., "Deep generative models for offline policy learning: Tutorial, survey, and perspectives on future directions," Trans. Mach. Learn. Res., 2024.
- [48] C. Li, et al., "Dof: A diffusion factorization framework for offline multiagent reinforcement learning," in Proc. Int. Conf. Learn. Represent. (ICLR), Singapore, Apr 2025.
- [49] Z. Zhu, et al., "Madiff: Offline multi-agent learning with diffusion models," in Proc. Adv. Neural Inf. Proces. Syst. (NeurIPS), Vancouver, Canada, Dec 2024, pp. 4177–4206.
- [50] J. Geng, et al., "Diffusion policies as multi-agent reinforcement learning strategies," in Proc. Int. Conf. Artif. Neural Netw., Heraklion, Crete, Greece, Sep 2023, pp. 356–364.

- [51] A. Kumar, et al., "Conservative q-learning for offline reinforcement learning," in Proc. Adv. Neural Inf. Proces. Syst. (NeurIPS), Virtual Edition, Dec 2020, pp. 1179–1191.
- [52] Z. Wang, et al., "Diffusion policies as an expressive policy class for offline reinforcement learning," in Proc. Int. Conf. Learn. Represent. (ICLR), Kigali, Rwanda, May 2023, pp. 26790–26807.
- [53] H. Lee, et al., "Convergence of score-based generative modeling for general data distributions," in Proc. Int. Conf. Algorithmic Learn. Theory (ALT), Singapore, Feb 2023.
- [54] S. Chen, et al., "Sampling is as easy as learning the score: theory for diffusion models with minimal data assumptions," in Proc. Int. Conf. Learn. Represent. (ICLR), Kigali, Rwanda, May 2023, pp. 30868– 30896.
- [55] J.-F. Le Gall, Brownian motion, martingales, and stochastic calculus. Springer, 2016.
- [56] H. Chen, et al., "Improved analysis of score-based generative modeling: User-friendly bounds under minimal smoothness assumptions," in Proc. Int. Conf. Mach. Learn. (ICML), Honolulu, Hawaii, USA, Jul 2023, pp. 4735–4763.
- [57] W. Stummer, "The novikov and entropy conditions of multidimensional diffusion processes with singular drift," *Probab. Theory Relat. Fields*, vol. 97, no. 4, pp. 515–542, 1993.
- [58] F. A. Oliehoek, et al., A concise introduction to decentralized POMDPs. Springer, 2016, vol. 1.
- [59] M. Janner, et al., "When to trust your model: Model-based policy optimization," in Proc. Adv. Neural Inf. Proces. Syst. (NeurIPS), Vancouver, Canada, Dec 2019, pp. 12519–12530.
- [60] Y. Song, et al., "Score-based generative modeling through stochastic differential equations," in Proc. Int. Conf. Learn. Represent. (ICLR), Virtual Edition, May 2021, pp. 240–276.
- [61] J. Ho, et al., "Denoising diffusion probabilistic models," in Proc. Adv. Neural Inf. Proces. Syst. (NeurIPS), Virtual Edition, Dec 2020, pp. 6840–6851
- [62] B. D. Anderson, "Reverse-time diffusion equation models," Stochastic Processes Appl., vol. 12, no. 3, pp. 313–326, 1982.
- [63] J. Ho, et al., "Classifier-free diffusion guidance," arXiv preprint arXiv:2207.12598, 2022.
- [64] P. Dhariwal, et al., "Diffusion models beat gans on image synthesis," in Proc. Adv. Neural Inf. Proces. Syst. (NeurIPS), Virtual Edition, Dec 2021, pp. 8780–8794.
- [65] H. T. Friis, "A note on a simple transmission formula," *Proc. IRE*, vol. 34, no. 5, pp. 254–256, May 1946.
- [66] K. Meng, et al., "Conditional diffusion model with OOD mitigation as high-dimensional offline resource allocation planner in clustered ad hoc networks," *IEEE Trans. Commun.*, 2025, early access.
- [67] H. E. Stanley, Phase transitions and critical phenomena. Clarendon Press, Oxford, 1971.
- [68] C. Allen, et al., "Learning markov state abstractions for deep reinforcement learning," in Proc. Adv. Neural Inf. Proces. Syst. (NeurIPS), Virtual Edition, Dec 2021, pp. 8229–8241.
- [69] Q. Hao, et al., "Gat-mf: Graph attention mean field for very large scale multi-agent reinforcement learning," in Proc. ACM SIGKDD Conf. Knowl. Discov. Data Min., Long Beach, California, USA, Aug 2023, pp. 685–697.
- [70] O. Ronneberger, et al., "U-net: Convolutional networks for biomedical image segmentation," in Proc. Med. Image Comput. Comput. Assist. Interv. (MICCAI), Munich, Germany, Oct 2015.
- [71] L. Pan, et al., "Plan better amid conservatism: Offline multi-agent reinforcement learning with actor rectification," in Proc. Int. Conf. Mach. Learn. (ICML), Baltimore, Maryland, USA, Jul 2022, pp. 17221–17237.
- [72] S. Fujimoto, et al., "A minimalist approach to offline reinforcement learning," in Proc. Adv. Neural Inf. Proces. Syst. (NeurIPS), vol. 34, Virtual Edition, Dec 2021, pp. 20132–20145.
- [73] L. Chen, et al., "Decision transformer: Reinforcement learning via sequence modeling," in Proc. Adv. Neural Inf. Proces. Syst. (NeurIPS), Virtual Edition, Dec 2021.
- [74] C. Lu, et al., "Dpm-solver: A fast ode solver for diffusion probabilistic model sampling in around 10 steps," in Proc. Adv. Neural Inf. Proces. Syst. (NeurIPS), New Orleans, Louisiana, USA, Nov 2022, pp. 5775– 5787.
- [75] K. Ito, et al., On stochastic differential equations. American Mathematical Society New York, 1951, vol. 4.
- [76] H. Risken, "Fokker-planck equation," in The Fokker-Planck equation: methods of solution and applications. Springer, 1989, pp. 63–95.